Frequency Effet of Transonic Flow Over an Oscillating Airfoil

By

Kiyoaki ONO*

(February 5, 1983)

Summary: A numerical study is presented for the transonic flow over a two-dimensional airfoil oscillating in pitch at the moderately high mean value of the angle of attack. Stressed is the understanding of the frequency effect on the surface pressure characteristics against the instantaneous angle of attack, due to the interaction between the shock-wave and the after-shock separated boundary layer. An implicit factored finite-difference method developed by Beam & Warming is applied to the compressible Navier-Stokes equations. The remarkable improvement of the computation speed is achieved with the program vectorization suitable for CRAY 1-S. The computational results are compared with the experimental data measured at the NASA-Ames 11-by-11 Foot Wind Tunnel.

1. Introduction

The understanding of the unsteady transonic flow over an oscillating airfoil is quite important for the analysis of the aerodynamic force on a helicopter rotor and of such dynamic phenomena as flutter and buffet. So extensive investigations, both experimentally and theoretically, have been conducted in various research institutes. (Ref. 1)

When the shock-wave formed on an airfoil surface is strong enough to induce the flow separation in the after-shock boundary layer, the proper analysis of the viscous/inviscid interaction is essential for the understanding of the flow field.

Beam & Warming (Ref. 2) showed an efficient finite-difference method for the Navier-Stokes equations in a conservation-law form. They used an implicit factorization scheme, in which a large time step was allowed to be taken. Steger (Ref. 3) combined their method and the body fitted grid generation system developed by Thompson, etc. (Ref. 4) for the analysis of the flow around an arbitrary-shaped body. The "thin layer" assumption was adopted and all the derivatives along the body surface in the viscous terms were neglected. Chyu, etc. (Ref. 5) developed an efficient time-varying grid generation technique suitable for the unsteady airfoil problem. This technique was added to Steger's program and they computed the flow around a NACA64A010 airfoil in pitch $\pm 1°$ at 0.25 chord with the mean value of the angle of attack 0°. The uniform flow Mach number M_∞ was 0.8 and the Reynolds number RE was 12×10^6. The reduced frequency $K=\omega c/2U$ was set on 0.2. The shock-wave formed on the airfoil surface was not so strong as to induce the flow separation. The agreement between the computational results due to both the inviscid and the viscous methods and the experimental data was

* Department of mechanical engineering college of science and technology Nihon University.

good. Chyu & Kuwahara (Ref. 6) added the viscous terms neglected in the previous calculations and applied their new program to the same problem as Chyu, etc. treated, except the mean valne of the angle of attack. It was 4°. The shock-wave was strong enough to induce the after-shock separation, and the full viscous calculation gave the best agreement with the experimental data.

The purpose of this report is, first of all, to show how much the computation time can be saved by properly vectorizing the program for CRAY 1-S at NASA-Ames Research Center. This vectorized program is used to compute the flow over a two-dimensional NACA64A010 airfoil in pitch $\pm 1°$ at 0.25 chord with the mean value of the angle of attack 4° in the uniform flow $M_\infty = 0.8$. The Reynolds number is 12×10^6. The lower frequency case $K = 0.05$ is newly computed. Comparison will be made with the experimental measurement conducted by Davis, etc. (Ref. 7). The discussion will be focused on the influence of the oscillation frequency of the airfoil on the surface pressure response characteristics against the angle of attack.

2. Numerical Technique

In this section a numerical techuique is described for computing the flow over an oscillating airfoil.

2–1. Fundamental Equations

The governing two-dimensional compressible Navier-Stokes equations in $\xi - \eta$

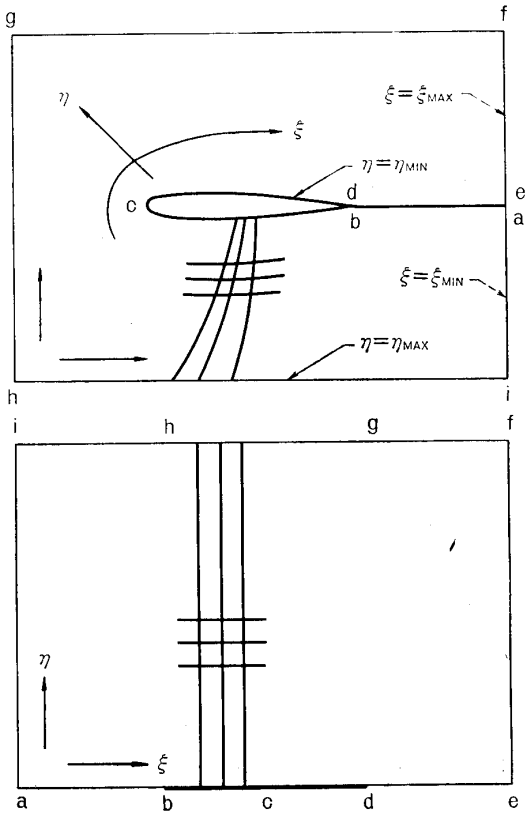

Fig. 1. Physical and Computatinal Planes.

body fitted coordinate system (Fig. 1) can be expressed in a conservation-law form as

$$\partial_\tau \hat{q}+\partial_\xi \hat{M}+\partial_\eta \hat{N}=0 \tag{1}$$

where

$$\hat{M}=\hat{E}-\frac{1}{RE}\hat{R}, \qquad \hat{N}=\hat{F}-\frac{1}{RE}\hat{S}. \tag{2}$$

Here, τ is the time variable and ξ & η mean the streamwise and the normal directions respectively. The flux vectors $\hat{q}$, $\hat{E}$, $\hat{F}$ are represented as

$$\hat{q}=\begin{bmatrix}\rho\\ \rho u\\ \rho u\\ e\end{bmatrix}, \qquad \hat{E}=\frac{1}{J}\begin{bmatrix}\rho U\\ \rho uU+\xi_x p\\ \rho vU+\xi_y p\\ (e+p)U-\xi_t p\end{bmatrix}, \qquad \hat{F}=\frac{1}{J}\begin{bmatrix}\rho V\\ \rho uV+\eta_x p\\ \rho vV+\eta_y p\\ (e+p)V-\eta_t p\end{bmatrix}. \tag{3}$$

The contravariant velocity components U & V are defined as

$$U=\xi=\xi_t+\xi_x u+\xi_y v, \qquad V=\eta_t+\eta_x u+\eta_y v. \tag{4}$$

The metric terms ξ_t, ξ_x, etc. and the transformation Jacobian $J=\xi_x\eta_y-\xi_y\eta_x$ are numerically determined at each time step. The viscous terms are

$$\hat{R}=\frac{1}{J}(\xi_x\vec{R}+\xi_y\vec{S}), \qquad \hat{S}=\frac{1}{J}(\eta_x\vec{R}+\eta_y\vec{S}) \tag{5}$$

where

$$\vec{R}=\begin{bmatrix}0\\ \tau_{xx}\\ \tau_{xy}\\ R_4\end{bmatrix}, \qquad \vec{S}=\begin{bmatrix}0\\ \tau_{xy}\\ \tau_{yy}\\ S_4\end{bmatrix} \tag{6}$$

with

$$\begin{aligned}
\tau_{xx}&=(\lambda+2\mu)u_x+\lambda v_y\\
\tau_{xy}&=\mu(u_y+v_x)\\
\tau_{yy}&=(\lambda+2\mu)v_y+\lambda u_x\\
R_4&=u\tau_{xx}+v\tau_{xy}+\alpha\partial_x a^2\\
S_4&=u\tau_{xy}+v\tau_{yy}+\alpha\partial_y a^2.
\end{aligned} \tag{7}$$

Here

$$a^2=\gamma(\gamma-1)\{e/\rho-\tfrac{1}{2}(u^2+v^2)\}, \qquad \alpha=kPr^{-1}(\gamma-1)^{-1} \tag{8}$$

with k & Pr denoting the thermal conductivity and the Prandtl number. γ is the specific heat ratio. The Stokes hypothesis $\lambda+\frac{2}{3}\mu=0$ is assumed.

The molecular viscosity μ is determined using the Sutherland law. For turbulent

flows the viscosity coefficients are computed using the two-layer zero equation model developed by Cebeci & Smith (Ref. 8) and improved by Baldwin & Lomax (Ref. 9).

2–2. Finite-Difference Algorithm

The Euler implicit finite-difference scheme represents the two-dimensional compressible Navier-Stokes equations in a conservation-law form as

$$\begin{aligned}\Delta\hat{q}^n=\hat{q}^{n+1}-\hat{q}^n&=\Delta\tau\left(\frac{\partial\hat{q}}{\partial\tau}\right)^{n+1}+O(\Delta\tau^2)\\&=-\Delta\tau\left\{\left(\frac{\partial\hat{M}}{\partial\xi}\right)^{n+1}+\left(\frac{\partial\hat{N}}{\partial\eta}\right)^{n+1}\right\}+O(\Delta\tau^2).\end{aligned}\tag{9}$$

The convection terms $\hat{E}$ & $\hat{F}$ in $\hat{M}$ & $\hat{N}$ are linearized using the local Taylor expansion about $\hat{q}$, that is,

$$\begin{aligned}\hat{E}^{n+1}&=\hat{E}^n+\left(\frac{\partial\hat{E}}{\partial\hat{q}}\right)^n\Delta\hat{q}^n+O(\Delta\tau^2)\\\hat{F}^{n+1}&=\hat{F}^n+\left(\frac{\partial\hat{F}}{\partial\hat{q}}\right)^n\Delta\hat{q}^n+O(\Delta\tau^2).\end{aligned}\tag{10}$$

The viscous term $\hat{S}$ can be divided into two parts, that is, $\hat{S}^\eta$ which consists of only η-derivative terms and $\hat{S}^\xi$ which involves ξ-derivative ones. The same linearization is applied to $\hat{S}^\eta$ as

$$\hat{S}^{\eta^{n+1}}=\hat{S}^{\eta^n}+\left(\frac{\partial\hat{S}^\eta}{\partial\hat{q}}\right)^n\Delta\hat{q}^n+O(\Delta\tau^2).\tag{11}$$

The other viscous terms $\hat{S}^\xi$ & $\hat{R}$ are lagged in time, giving an explicit expressions

$$\hat{S}^{\xi^{n+1}}=\hat{S}^{\xi^n}+O(\Delta\tau),\qquad\hat{R}^{n+1}=\hat{R}^n+O(\Delta\tau).\tag{12}$$

Such simplification is allowed because the η-spacing $\Delta\eta$ is much finer than the ξ-spacing $\Delta\xi$, so only the η-derivative terms should be estimated implicitly for the numerical stability improvement. Using these approximations Equs. (10)–(12), Equ. (9) can be expressed as

$$\begin{aligned}&\left(I+\Delta\tau\frac{\partial}{\partial\xi}\left(\frac{\partial\hat{E}}{\partial\hat{q}}\right)^n\right)\left(I+\Delta\tau\left(\frac{\partial}{\partial\eta}\frac{\partial}{\partial\hat{q}}\left(\hat{F}-\frac{1}{RE}\hat{S}^\eta\right)^n\right)\right)\Delta\hat{q}^n\\&\quad=-\Delta\tau\left(\frac{\partial}{\partial\xi}\hat{M}+\frac{\partial}{\partial\eta}\hat{N}\right)^n+(\Delta\tau^2)\end{aligned}\tag{13}$$

where I is the unit matrix. The term $\tilde{q}$, defined as

$$\tilde{q}=\left(I+\Delta\tau\frac{\partial}{\partial\eta}\frac{\partial}{\partial\hat{q}}\left(\hat{F}-\frac{1}{RE}\hat{S}^\eta\right)^n\right)\Delta\hat{q}^n,\tag{14}$$

can be calculated as

$$\tilde{q}=-\Delta\tau\left(I+\Delta\tau\frac{\partial}{\partial\xi}\left(\frac{\partial\hat{E}}{\partial\hat{q}}\right)^n\right)^{-1}\left(\frac{\partial}{\partial\xi}\hat{M}+\frac{\partial}{\partial\eta}\hat{N}\right). \tag{15}$$

Then $\Delta\hat{q}^n$ is obtained from the following equation,

$$\Delta\hat{q}^n=\left(I+\Delta\tau\left(\frac{\partial}{\partial\eta}\frac{\partial}{\partial\hat{q}}\left(\hat{F}-\frac{1}{RE}\hat{S}^\eta\right)^n\right)\right)^{-1}\cdot\tilde{q}. \tag{16}$$

So the value $\hat{q}$ at time step $n+1$ is computed as

$$\hat{q}^{n+1}=\hat{q}^n+\Delta\hat{q}^n. \tag{17}$$

In the present study the space derivative terms are replaced by the central difference method, so the accuracy of this scheme is first order in time and second one in space.

2–3. Boundary Condition

On the airfoil surface, the no-slip condition is required for the viscous flow, that is,

$$U=V=0. \tag{18}$$

The density ρ is determined from the extrapolation of the value at the grid points next to the body surface. The pressure p is computed by solving the normal momentum equation. The uniform flow conditions are imposed for the far-away boundary except the downstream one, where the flow quantities at the grid points just inside the boundary is extrapolated.

2–4. Grid Generation

For an oscillating airfoil problem, the grid points must be determined at each time step. So to save the computation time, the grid points at the extreme angle of attack positions are first generated using Thompson's method (Ref. 4). Then the grid points at the intermediate angle of attack are determined by linear interpolation. An example of the generated grid system is shown in Fig. 2. The grid spacings in the η-directions are clustered in the boundary layer so that the adequate resolution for the viscous flow analysis is assured. The finer grid points are distributed near the leading and the trailing edges along the ξ-direction.

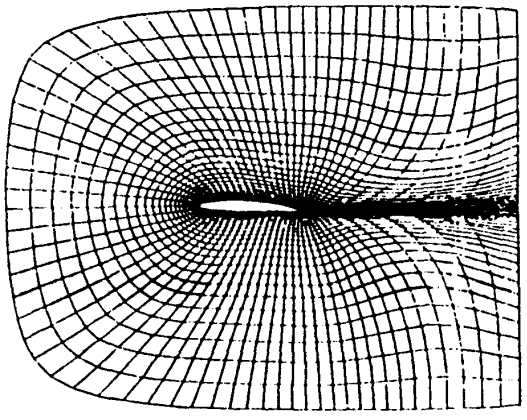

Fig. 2. An Example of Generated Grids.

3. Results

The present study is the extension of Ref. 6 and focused on the investigation of the frequency effect on the shock-wave/boundary layer interactions, which decide the surface pressure response characteristics against the instantaneous angle of attack. So the computation is carried out for the unsteady flow over a two-dimensional NACA64A010 airfoil oscillating in pitch at 0.25 chord with the mean value of the angle of attack 4° in the uniform flow $M_\infty=0.8$. The mesh size is 87×41 in ξ and η directions respectively. In Ref. 6 the higher oscillation frequency case, where the reduced frequency K is 0.2, is reported. The lower frequency case ($K=0.05$) will be added in this report.

3–1. Experimental Measurement

A series of experimental measurements have been conducted by Davis, etc. (Ref. 7) at NASA-Ames 11-by-11 Foot Transonic Wind Tunnel. A conventional NACA64A010 and a supercritical NLR7301 airfoils undergo pitching or plunging oscillation and time history of surface pressure variation was measured. The data will be compared in the following sections with the computational results.

3–2. Computation Speed

The computation speeds of CDC 7600 and CRAY 1–S are compared in Table 1. The computation time required to proceed one time step and to complete one full cycle are shown. In this case one cycle is devided into 2160 steps. CRAY 1–S's computation speed is only twice than that of CDC 7600's when the same FORTRAN program originally written for CDC 7600 is run in CRAY 1–S. But if the program is carefully vectorized, its computation speed is ten times faster than the original one.

Table 1. Comparison of computation speed

	CDC 7600	CRAY (no vect.)	CRAY (vect.)
Time/Iteration	4.6 sec.	2.0 sec.	0.25 sec.
Time/Cycle	165 min	72 min	9 min

3–3. Surface Pressure Variation

Computed instantaneous surface pressure distributions based on the inviscid (neglected all the viscous terms), the thin layer (retained only η-derivatives in the viscous terms) and the full viscous (computed all the viscous terms) assumptions are shown in Fig. 3. These computed results are for the higher frequency case ($K=0.2$) and refered from Ref. 6. Also shown in Fig. 3 is the experimental data. The fast pressure recovery after the shock location on the upper surface means the attached flow while the angle of attack is increasing. When it is around 4.87°, formed is the after-shock pressure bump, which shows that the flow in the boundary layer is separated. While the angle of attack is decreasing,

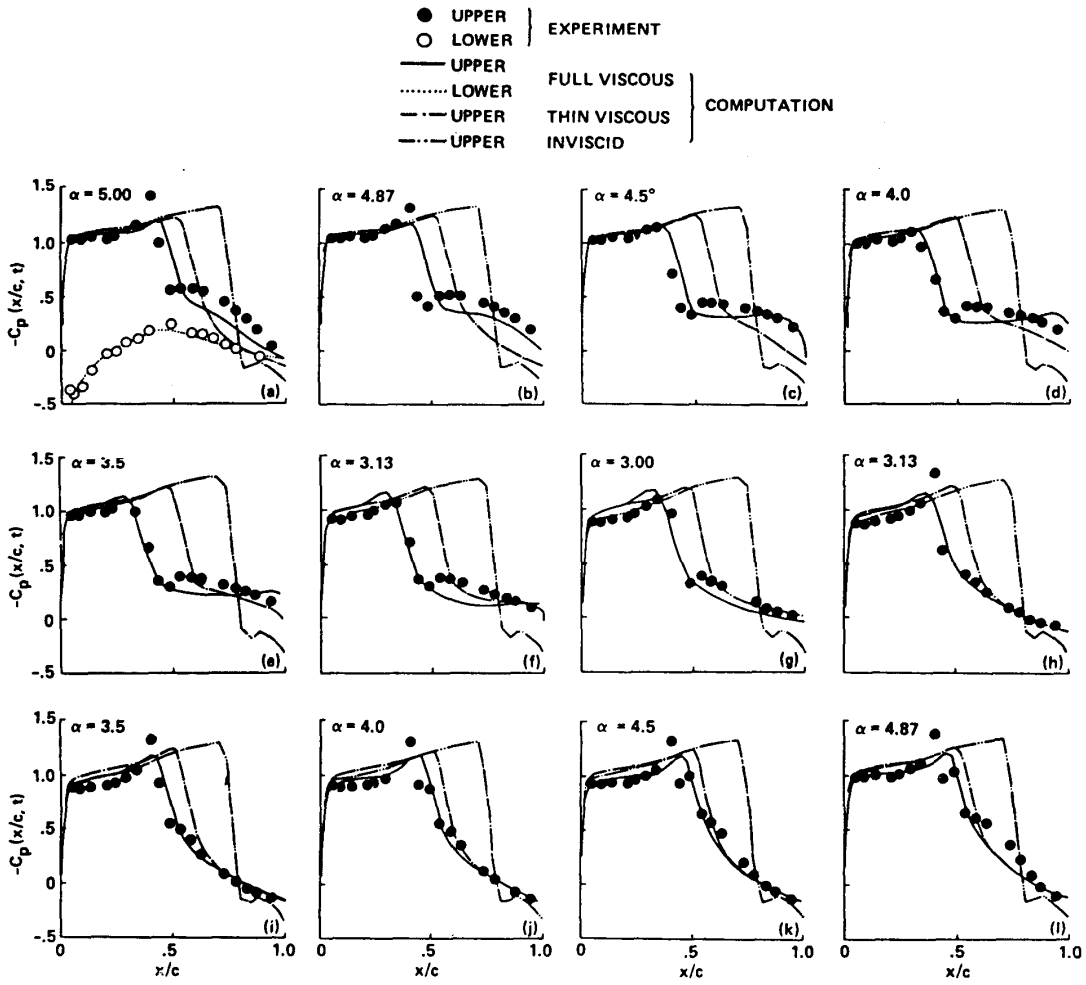

Fig. 3. Instantaneous surface Pressure Distributions (K=0.2).

the flow continues separated. It reattaches when the angle is around 3.13°. Judging from the shock location and the after-shock pressure distributions, it is concluded that the full viscous computation gives the best agreement with the experimental data. The thin layer computation predicts fairly well the fast pressure recovery portion but poor the slow recovery one. The inviscid computation entirely fails to predict the after-shock pressure distributions, which is strongly affected by the shock/boundary layer interactions.

3–4. Shock Locus

The loci of the shock location versus the angle of attack are shown for both frequency cases in Fig. 4. As far as the higher frequency case is concerned, the shock-wave formed on the upper surface moves downstream during the upward movement of the airfoil, but starts to move upstream at about 4.8° due to the occurrence of flow separation in the after-shock boundary layer. For the lower frequency case, on the contrary, the experimental measurement shows that the shock-wave moves upstream with increasing the angle of attack and downstream with its decrease. The computational result shows the same characteristics of the shock movement, but it contains the higher harmonic oscillation. The experimental

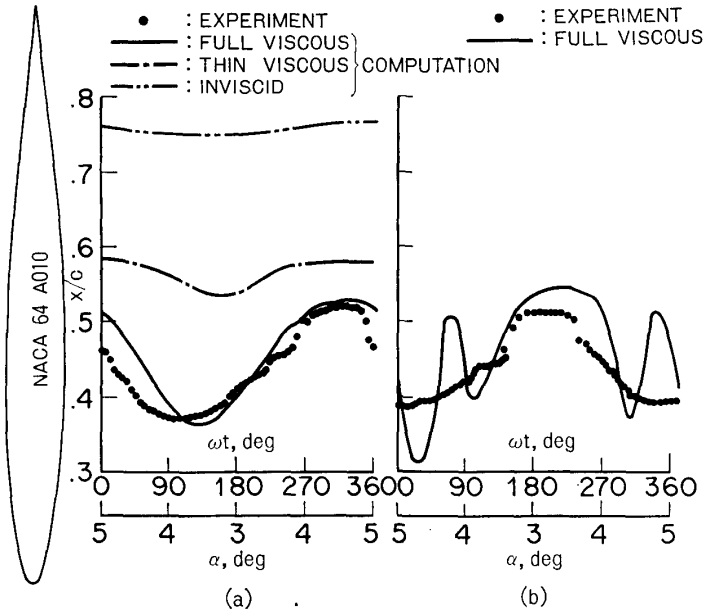

Fig. 4. Shock Loci on the Airfoil Surface.
(a) $K=0.2$, (b) $K=0.05$

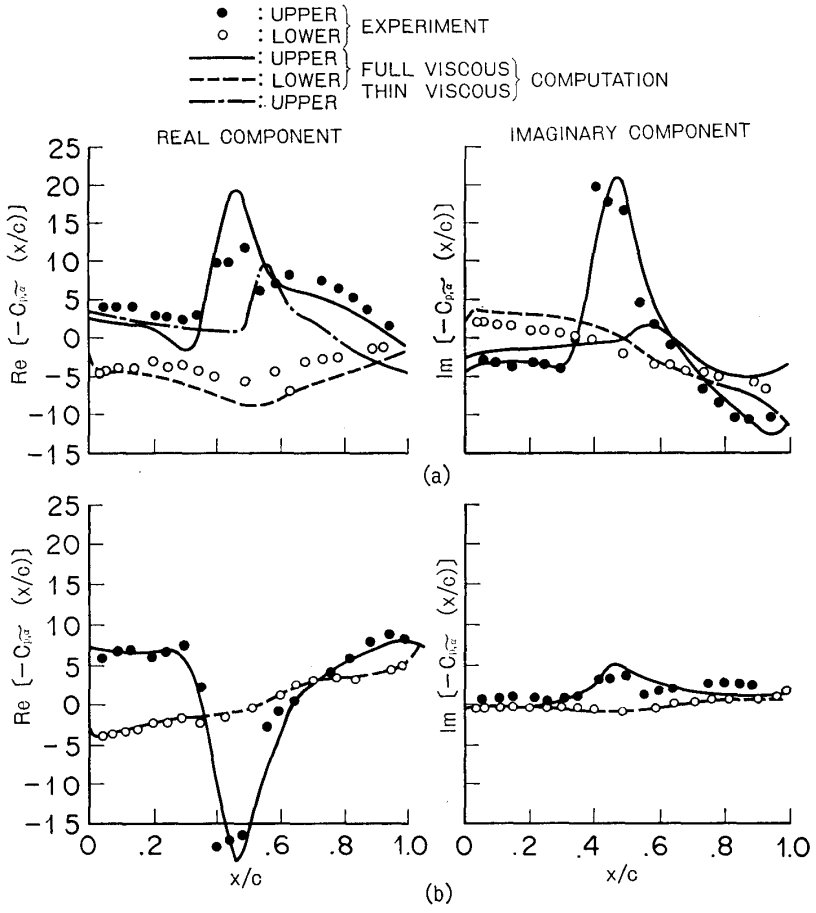

Fig. 5. Response Characteristics of the Airfoil Surface Pressure (Fundamental Mode).
(a) $K=0.2$, (b) $K=0.05$

data is the ensumble average of many samples. If the timing of shedding vortex is different on each sample, such higher harmonics should disappear in the experimental data. At the present stage there's no way to know if the higher harmonic vortex shedding actually occures or not.

3–5. Response Characteristics of the Airfoil Pressure

The response characteristics of the airfoil surface pressure to the airfoil motion is investigated using Fourier transformation. Suppose the instantaneous angle of attack α is expressed as

$$\alpha=\alpha_m+\mathrm{Re}(\tilde{\alpha}e^{i\omega t}), \tag{19}$$

the Fourier representation of the pressure coefficients can be written as

$$C_p(\chi/c,\ \tau)=C_{pm}(\chi/c)+\sum_{n=1}^{\infty}\mathrm{Re}(C^n_{p,\tilde{\alpha}}(\chi/c)\tilde{\alpha}e^{in\omega t}). \tag{20}$$

Here α_m is the mean value of the angle of attack. C_{pm} is the mean value of the pressure coefficient, and $C^n_{p,\tilde{\alpha}}$ is the n-th complex component of the pressure coefficient per radian. The real and the imaginary parts of the first harmonic components for both frequency cases are shown in Fig. 5. The comparison is also made with the experimental data. Both the real and the imaginary components have positive peaks on the upper surface pressure response distribution for the higher frequency case. The lower frequency case shows the negative peak on the real component. The numerical computation agrees well with the experimental one, and predicts that the respone characteristics of the surface pressure changes remarkably depending on the oscillation frequency.

4. Conclusion

The advance of the computer machine and the finite-difference technique has made possible the viscous computation of the transonic flow over an oscillating airfoil within the reasonable computer time. Made is the comparison of the pressure response characteristics against the angle of attack for the higher and the lower frequency cases ($K=0.2$ & 0.05) of a NACA64A010 airfoil oscillating in pitch $\pm1°$ at 0.25 chord in the uniform flow $M_\infty=0.8$. The mean value of the angle of attack is 4° and the Reynolds number is 12×10^6. The shock wave formed on the airfoil surface is strong enough to induce the separation in the after-shock boundary layer. Only the full viscous computation agrees well with the experimental data and shows clearly the difference of the response characteristics of the surface pressure, depending on the oscillation frequency.

Acknowledgment

This research was carried out under the supervise of Dr. W. J. Chyu at NASA-Ames Research Center, while the author was staying there as a NRC Research Associate.

References

[1] W. J. McCroskey: "Unsteady Airfoils," Annual Review of Fluid Mechanics, Vol. 14, 1982, pp. 285–311.

[2] B. Beam & R. F. Warming: "An Implicit Factored Scheme for the Compressible Navier-Stokes Equations," AIAA Journal, Vol. 16, 1978, pp. 393–402.

[3] J. L. Steger: "Implicit Finite-Difference Simulation of Flow about Arbitrary Two-Dimensional Geometries," AIAA Journal, Vol. 16, 1978, pp. 679–686.

[4] J. F. Thompson, etc.: "Automatic Numerical Generation of Body-Fitted Curvilinear Coordinate System for Field Containing any Number of Arbitrary Two-Dimensional Bodies," Journal of Computational Physics, vol 15, 1974, pp. 299–319.

[5] W. J. Chyu, etc.: "Calculation of Unsteady Transonic Flow over an Airfoil," AIAA Journal, Vol. 19, 1981, pp. 584–690.

[6] W. J. Chyu & K. Kuwahara: "Computation of Transonic Flow over an Oscillating Airfoil with Shock-Induced Separation," AIAA Paper 82-350, 1982.

[7] S. S. Davis, etc.: "Transonic Shock-Wave/Boundary-Layer Interactions on an Oscillating Airfoil," AIAA Journal, Vol. 18, 1980, pp. 1306–1312.

[8] T. Cebeci & A. M. O. Smith: "Analysis of Turbulent Boundary Layers," Academic Press, 1974.

[9] B. S. Baldwin & H. Lomax: "Thin Layer Approximation and Algebraic Model for Separated Turbulent Flow," AIAA Paper 78-257, 1978.